Comparison of the influence of silica-rich supplementary cementitious materials on cement mortar composites: Mechanical and microstructural assessment

Ozer Sevim (ozersevim@kku.edu.tr)
Kırıkkale Üniversitesi https://orcid.org/0000-0001-8535-2344
Cagrı Goktug Sengul
Kirikkale University: Kirikkale Universitesi

Original Research

Keywords: Cement mortar composites, Supplementary cementitious materials (SCMs), Microstructure, Blast furnace slag, Fly ash, Bottom ash, Blaine fineness, Compressive strength

Posted Date: February 2nd, 2021

DOI: https://doi.org/10.21203/rs.3.rs-157559/v1

Version of Record: A version of this preprint was published at Silicon on February 18th, 2021. See the published version at https://doi.org/10.1007/s12633-021-01013-7.

Abstract

The silica-rich supplementary cementitious materials (SCMs) are the key components of mechanical and microstructural properties. The use of SCMs results in improving the mechanical and microstructural properties and decreasing the environmental burden caused by cement production. In this regard, this paper reports a study to compare the influence of silica-rich supplementary cementitious materials (slag, fly ash, and bottom ash) having similar Blaine fineness on cement mortar composites in terms of mechanical and microstructural properties. First, supplementary cementitious materials (slag, fly ash, and bottom ash) were ground at similar cement Blaine fineness (~ 3300 cm^2/g) and then by replacing 5% and 20% with cement, the 7-, 28-, 90-day mechanical and microstructural properties of cement mortar composites incorporating SCMs were examined. As a result, it was observed that the compressive strength and microstructural properties of cement mortar composites incorporating slag gave maximum strength and microstructural properties according to samples with fly ash and bottom ash having similar fineness and this will decrease the required amount of cement for the target properties by using slag, thus the number of CO_2 emitted to nature will also decrease.

1. Introduction

Supplementary cementitious materials (SCMs), including fly ash, ground granulated blast furnace slag, bottom ash, silica fume, etc., are widely used in clinker to make Portland cement or added as a replacement for a portion of ordinary Portland cement in concrete [1–6]. This is due to the potential capability of supplementary cementitious materials to increase the properties of concrete through their filler effect, as well as pozzolanic reaction. In addition, most of the SCMs are by-product materials; hence, the use of by-products prevents the destruction of the non-renewable resources by hindering the use of very limited natural materials and minimizes environmental problems by the disposal of waste [7–8]. Concrete is of great importance for the evaluation of industrial by-products. Currently, concrete is widely used with more than 10 billion tons produced annually in the world [9]. The amount of CO_2 gas released to nature during production increases. The cement industry is responsible for about 7% of the total CO_2 emissions in the world. It has been shown that every ton of ordinary Portland cement manufactured emits almost one ton of CO_2 into the atmosphere [10–11]. One of the main methods of reducing this emission is to keep the properties of cement as a building material and to substitute industrial by-products with the cement. Their utilization in concrete can serve as an effective means of disposal. Moreover, their utilization as supplementary cementitious materials to partially replace cement could protect the natural resources needed to produce cement and thus can contribute to sustainable concrete manufacture.

Supplementary cementitious materials are defined as materials containing high levels of silica and alumina, which do not have binding properties on their own but have hydraulic binding properties when combined with water and calcium hydroxide (CH) [12–13]. The blast furnace slag, fly ash, bottom ash represents the majority of supplementary cementitious materials. The utilization of supplementary cementitious materials as a component of concrete happened to ordinary [14–23]. It has been shown in

the literature that the use of supplementary cementitious materials as cement additive improves the mechanical and durability properties of concrete [24–26]. These improvements depend on the different properties of the supplementary cementitious materials. One of these properties is the Blaine fineness of supplementary cementitious materials. Research examining the effect of Blaine fineness of supplementary cementitious materials on cementitious composites is available in the literature.

Bentz et al. investigated the effect of fly ash Blaine fineness as a supplementary cementitious material in their studies. The compressive strength of the samples containing fly ash with higher Blaine fineness was higher than the reference mixture containing 100% Portland cement [27–28]. Slanicka (1991) [29] explored the effect of utilization of fly ash as supplementary cementitious material in concrete with different Blaine fineness on mechanical properties. In their study, the Blaine fineness led to prominent differences in the mechanical properties of concrete. Zhang et al. (2004) [30] substituted 50% of the ground blast furnace slag to cement having Blaine fineness 3460 and 8380 cm^2/g. It was showed that ground granulated blast furnace slag having higher Blaine fineness has higher mechanical properties. Li and Zhao (2003) [31] produced high strength concrete by ground blast furnace slag and ground fly ash in different ratios and Blaine fineness adding them to cement as an additive. As a result, it has been shown that the composites in which ground blast furnace slag and ground fly ash gave positive effects both in the short term and in the long term. Monzo et al. (1994) [32] investigated the mechanical properties of cement mortar composites incorporating fly ash with different Blaine fineness at a 30% replacement ratio. They stated that the mechanical properties increased with the increase of fly ash fineness. Sevim and Demir (2019) [33–34] and Filazi et al. (2020) [35] explore that the mechanical and durability properties of cement mortar composites with fly ash replacement with help of particle size distribution of fly ash. They stated that all properties increased with the increase of fly ash fineness with the help of particle size distribution. Karim et al. (2020) [36] showed that strength development of alkali-activated binder-mortar is greatly influenced by the types and fineness of SCMs. Ma et al. (2020) [37] observed that the pozzolanic activity increases with increasing waste brick powder fineness. Alaskar et al. (2020) [38] showed that increased fineness of the silica fume blended cement increased the compressive strength of concrete. Shaikh and Arel (2020) [39] showed that the compressive strength of steel fiber reinforced concrete increase with the increase in fly ash fineness. Sun et al. (2020) [40] indicate that the compressive strength increases linearly with the increase of fly ash fineness. Maeijer et al. (2020) [41] showed that an increased fineness of fly ash contributes to better strength, durability and workability. Hallet et al. [42] showed that an increased fineness of blast furnace slag did not yield significant compressive strength enhancement at early ages, but the increased reactivity for higher slag fineness led to more hydration products and consequently higher compressive strengths at 28 days. Khongpermgoson et al. (2020) [43] showed that grinding coal bottom ash improved its quality by achieving high fineness, and it increased strength.

Having carried out a thorough literature review, to date, existing studies only focused on the influence of different fineness of some kind of supplementary cementitious materials on cement-based composite properties. To address the above-mentioned research gap, this paper reports a study to compare the

influence of silica-rich supplementary cementitious materials (slag, fly ash, and bottom ash) having similar Blaine fineness on cement mortar composites in terms of mechanical and microstructural properties. In this regard, supplementary cementitious materials (slag, fly ash, and bottom ash) were ground at similar cement Blaine fineness (~ 3300 cm^2/g) and then by replacing 5% and 20% with cement, the 7-, 28-, 90-day mechanical and microstructural properties of cement mortar composites incorporating SCMs were examined. The findings of the present study contribute significantly to the understanding of how to improve mechanical and microstructural properties in the development of cement mortar composites using more SCM with the help of increased fineness.

2. Experimental Program

2.1. Materials

2.1.1. Cement, blast furnace slag, fly ash, and bottom ash.

In this study, CEM I 42.5 R type ordinary Portland cement (OPC) in accordance with EN 197-1 [44], ground granulated blast furnace slag (GGBFS) obtained from Eregli Iron and Steel Plant (in Eregli, Turkey), fly ash (FA) and bottom ash (BA) obtained from Catalagzı Thermal Power Plant (in Zonguldak, Turkey) were used. Bottom ash was calcined at 1000˚C to minimize the carbon content. The SCMs used were ground in a ring mill and the specific gravity and specific surface area of the SCMs were calculated in the laboratory. The physical and chemical properties of the OPC, GGBFS, FA, and BA are given in Table 1. Minor oxides were not considered in chemical oxide analysis.

Table 1
Chemical and physical properties of Portland cement, GGBFS, FA and BA

Chemical properties (%)	OPC	GGBFS	FA	BA
SiO_2	21.05	36.10	44.69	42.35
Al_2O_3	5.31	10.67	11.13	15.41
Fe_2O_3	3.07	0.99	9.35	9.30
CaO	63.78	39.60	16.89	15.35
MgO	1.44	5.44	6.66	5.37
Na_2O	0.39	0.28	2.14	0.79
K_2O	0.88	1.18	4.12	1.24
SO_3	3.31	1.90	2.57	5.21
Physical properties				
Specific gravity	3.20	2.94	2.20	2.07
Blaine fineness (cm^2/g)	3330	3335	3295	3380
Loss on ignition (%)	2.21	2.10	1.07	5.21

2.1.2 Sand

The sand used in this study is the CEN reference sand specified in EN 196-1 [45] standard.

2.2 Methods

2.2.1. Mixture proportions

The sample coding and mixture design of the cement mortar composites incorporating SCMs are given in Table 2. To assess the hydration degree of the supplementary cementitious materials are used at replacement level 20% [46–48], in this regard, a 20% replacement ratio was used in this present study. Also, the effect of a 5% replacement ratio was assessed in this study.

Table 2
The sample coding and mixture design of cement mortar composites incorporating SCMs.

Additive Ratio (%)	Code	Cement (g)	Sand (g)	Water (g)	SCMs (g)
0	Control	450	1350	225	0
5	GGBFS 5	427.50	1350	225	22.50
20	GGBFS 20	360.00	1350	225	90.00
5	FA5	427.50	1350	225	22.50
20	FA20	360.00	1350	225	90.00
5	BA5	427.50	1350	225	22.50
20	BA20	360.00	1350	225	90.00

2.2.2. Test for compressive strength

The compressive strength tests were carried out complying with EN 196-1 [45]. The mixture ratios given in Table 2 were used for the preparation of cement mortar composites incorporating SCMs. For compressive strength testing, prismatic specimens measuring 40×40×40 mm were produced and initially cured at 7-, 28-, and 90-day. For measuring compressive strength prismatic samples were loaded at a loading rate of 2.4 kN/s and results of the compressive test results of six samples were averaged to find final values.

2.3. Test for microstructure analysis

The microstructural properties of cement mortar composites incorporating SCMs kept in water curing were examined at 7, 28, and 90 days and at 5% and 20% ground granulated blast furnace slag, fly ash, and bottom ash replacement ratio. Microstructures were examined with the help of a scanning electron microscope. For performing the microstructure surface inspection, specimens were applied gold coating with Sputter Coater. The specimens were investigated by scanning electron microscopy. Scanning Electron Microscope (SEM) image is obtained by collecting the effects of elastic and inelastic collisions between electrons and sample atoms during scanning of the electron beam accelerated by high voltage and focused on the sample on the sample surface, passing through the signal amplifiers and transferring it to the screen of the cathode ray's tube.

3. Results And Discussion

3.1. Compressive strength

The compressive strengths at 7-, 28-and 90-day cement mortar composites incorporating slag, fly ash, and bottom ash with similar Blaine fineness at 5% and 20% replacement ratio were explored and are given in Table 3.

Table 3
The compressive and flexural strengths at 7-, 28- and 90-days old cement mortar composites incorporating GGBS, FA, and BA with similar Blaine fineness.

Samples	Compressive strength (MPa)		
	7-day	28-day	90-day
Control	35.65	46.60	54.43
FA5	34.22	45.77	54.15
FA20	30.51	41.88	53.23
BA5	33.78	42.60	53.44
BA20	30.05	41.17	50.74
GGBS5	34.36	45.98	54.21
GGBS20	32.23	43.17	53.87

When the percentage change of compressive strengths at 7 days cement mortar composites incorporating SCMs were examined, the percentage change of compressive strength results of the GGBFS5, FA5, BA5 samples with 5% replacement ratio were found 3.6%, 4.0%, and 5.3% lower than the control sample (35.65 MPa), respectively. At 7 days old samples with a 5% replacement ratio, the highest compressive strength result was observed in samples with slag and the lowest compressive strength result was observed in samples with bottom ash replacement. The percentage change of compressive strength results of GGBFS20, FA20, BA20 samples with a 20% replacement ratio were found 9.6%, 14.4%, and 15.7% lower than the control sample, respectively. At 7 days old samples with a 20% replacement ratio, the highest compressive strength result was observed in samples with slag replacement, and the lowest compressive strength was observed in samples with bottom ash. When the percentage change of compressive strengths at 28 days cement mortar composites incorporating SCMs were examined, the percentage change of compressive strength results of the GGBFS5, FA5, BA5 samples with 5% replacement ratio were found 1.3%, 1.8%, and 8.6% lower than the control sample (46.60 MPa), respectively. At 28 days old samples with a 5% replacement ratio, the highest compressive strength result was observed in samples with slag and the lowest compressive strength result was observed in samples with bottom ash replacement. The percentage change of compressive strength results of GGBFS20, FA20, BA20 samples with a 20% replacement ratio were found 7.4%, 10.1%, and 3.4% lower than the control sample, respectively. At 28 days old samples with a 20% replacement ratio, the highest compressive strength result was observed in samples with slag replacement, and the lowest compressive strength was observed in samples with bottom ash. When the percentage change of compressive strengths at 90 days cement mortar composites incorporating SCMs were examined, the percentage change of compressive strength results of the GGBFS5, FA5, BA5 samples with 5% replacement ratio were found 0.4%, 0.5%, and 1.8% lower than the control sample (54.43 MPa), respectively. At 90 days old samples with a 5%

replacement ratio, the highest compressive strength result was observed in samples with slag and the lowest compressive strength result was observed in samples with bottom ash replacement. All results were similar at 90 days samples at a 5% replacement ratio. The percentage change of compressive strength results of GGBFS20, FA20, BA20 samples with a 20% replacement ratio were found 1.0%, 2.2%, and 6.8% lower than the control sample, respectively. At 90 days old samples with a 20% replacement ratio, the highest compressive strength result was observed in samples with slag replacement, and the lowest compressive strength was observed in samples with bottom ash.

When the compressive strength results of cement mortar composites incorporating slag, fly ash, and bottom ash with similar Blaine fineness are explored, the compressive strength of the composites incorporating slag gave the highest results, followed by composites incorporating fly ash and the lowest results has been observed composites incorporating bottom ash. When looking at the chemical properties of these SCMs substituting into cement, it is necessary to evaluate the components of SiO_2 and calcium oxide (CaO), providing the formation of C_3S, C_2S, which play a major role in the cement's binding property and the formation of its first and final strength. The use of SCMs with low calcium content generally decreases the mechanical strength of cement mortar composites at early ages when compared to cement mortar composites without additives. On the other hand, the use of SCMs with high-calcium content has a positive effect on strength development. The use of supplementary cementitious materials with low calcium content usually reduces the mechanical strength of cementitious composite systems at early ages when compared to cementitious composites without additives. On the other hand, the use of supplementary cementitious materials with high-calcium content has a positive effect on strength development [49–51]. Note that the calcium oxide (CaO) amounts of slag, fly ash and bottom ash are 39.60%, 16.89%, 15.35%, respectively and the amount of SiO_2 in the chemical structure of these SCMs is 36.10%, 44.69%, and 42.35% for slag, fly ash and bottom ash, respectively. Although the material with the highest amount of SiO_2 is fly ash, due to the low amount of calcium oxide (CaO), it could not contribute to the formation of C_3S and C_2S as much as slag. Therefore, the compressive strength results of composites with slag replacement are higher than composites incorporating fly ash and bottom ash replacement with similar Blaine fineness. The cementing ability of slag is very high, and it has the highest specific gravity, therefore it gave the best results. In addition, the fact that the SiO_2 and CaO amounts of the composites incorporating fly ash were higher than the composites incorporating bottom ash, causing the strength results of the composites incorporating fly ash to be higher than the composites having bottom ash replacement. Note that the highest loss on ignition is 5.21, which is in bottom ash, so the lowest mechanical results are found in cement mortar composites incorporation bottom ash.

3.2. Microstructure analysis

The microstructural properties of cement mortar composites incorporating SCMs were examined at 7, 28, and 90 days and at 5% and 20% slag, fly ash, and bottom ash replacement ratio. Microstructures were examined with the help of a scanning electron microscope.

Cement mortar composites have hydration products such as calcium silicate hydrate (C-S-H), calcium hydroxide (CH), and ettringite (C-A-S-H) in their microstructure. Calcium silicate hydrate gels are the most important phase affecting the properties of cement paste with the progress of the hydration process. The morphological structure of C-S-H gel is that they gain a web-like structure from weak crystalline fibers. In the early stages of the hydration process, C-S-H gels develop into water-filled spaces by forming thin layers of low density. During the hydration process, C-S-H concentrates around the hydrated cement particles and covers all particles. CH morphology has a structure that varies structurally from a generally undefined shape to a cluster of large plaques. Compared to C-S-H gels, it contributes less to strength due to its low surface area.

Calcium silicate hydrate (C-S-H), calcium hydroxide (CH) developments of microstructure studies of cement mortar composites incorporating slag, fly ash, bottom ash samples, and control samples were investigated by scanning electron microscope at 2000× and 5000× magnifications.

3.2.1. Microstructure analysis of additive-free samples

7-day SEM images of the samples without additive are given in Fig. 4. It was observed in the images that C-S-H gels started to develop at 7-day-old samples at 2000× and 5000× magnifications and CH gels were formed. It is seen that the density of C-S-H in the samples started to increase and developed by covering the CH gels. CH gels reach 20 μm in size, while C-S-H gels with 10 μm dimensions are in the first development process in the early strength process.

SEM images of the samples at 28 days are given in Fig. 5. When the images are examined, it is seen that the C-S-H gels reach a web-like structure and cover the entire surface. The CH gels in the structure are covered with the web-like structure of C-S-H gels. C-S-H gels fill the gaps in the cement mortar composites during the hydration process. At the 2000× and 5000× images of the samples, the web-like structure of the C-S-H gels was seen in Fig. 5 to fill the void structure in the cement mortar composites. C-S-H gels observed at 5000× magnification at 7-day images of the samples at a size of 2 μm reach approximately ranges from 20 to 25 μm at 28-day samples and cover the entire structure.

SEM images of the samples at 90 days are given in Fig. 6. In the images, it is seen that the web-like structure of the developed C-S-H gels has completely developed, and the structures have increased to 30 μm and above and this web-like structure completely covers the microstructure of the cement mortar composites.

Developments in the microstructure of cement directly affect the strength and durability properties of cement mortar composites. The increase in the formation of dense C-S-H gels in the samples without additives due to the curing time causes the compressive strength to increase depending on the curing time.

3.2.2. Microstructure analysis of samples having GGBFS.

Microstructure analysis of the slag added samples were performed at 7-, 28- and 90-days curing times according to 5% and 20% replacement ratio. SEM images at 7-day samples with a 5% slag replacement rate at 2000× and 5000× magnification is given in Fig. 7. When the images are examined, it is seen that the web-like structure of the C-S-H gels is formed and begins to condense on the surface. The fibrous C-S-H gels that filled the gaps reached a size of approximately ranges from 5 to 10 μm.

SEM images of the samples with the same replacement ratio at 28-day at 2000× and 5000× magnification is given in Fig. 8. When these images are examined, it is seen that the density of C-S-H gels has increased compared to 7-day samples and completely covers the structure. C-S-H gels developed in the form of a web, completely filling the void structures and reached a size of approximately 20 μm.

SEM images obtained at 2000× and 5000× magnification at 90-day samples with a 5% slag replacement ratio are given in Fig. 9. When the images are evaluated, C-S-H gels are partially seen size of approximately ranges from 30 to 40 μm, and it is seen that the ettringite needles are concentrated and reached a size of approximately 50 μm.

SEM images of the samples with 20% slag replacement ratio at 7, 28, and 90 days at 2000× and 5000× magnification are given in Fig. 10, Fig. 11, and Fig. 12, respectively. When the SEM images were examined, it was observed that fibrous C-S-H gels developed and started to condense at 7-day-old samples. It has been observed that the web-like structures formed by the gels develop in a size of approximately ranges from 5 to 10 μm.

At the 28-day SEM images of the samples with the same replacement ratio, it was observed that the C-S-H gels covered the entire structure, developed in the voids and the web-like C-S-H structure developed and took the form of a cactus. The cactus shaped C-S-H phase has reached the size of about 20 μm. The development of the gels increased compared to 7-day samples.

When the 90-day SEM images were examined, it was seen that C-S-H gels and ettringite needles covered the entire structure. C-S-H gels and ettringite needles were observed to be range from 30 to 40 μm at 5000× magnification.

3.2.3. Microstructure analysis of samples having FA.

Microstructure studies were carried out at 7-, 28- and 90-days curing times according to 5% and 20% replacement ratio of fly ash substituting samples. SEM images at 7-day samples with a 5% fly ash replacement ratio, at 2000× and 5000× magnification, are given in Fig. 13. When the images are examined, it is seen that the web-like structure of the C-S-H gels started to form. The gels that started to fill the gaps reached a size of approximately 5 μm.

SEM images of the samples with the same replacement ratio at 28 days, at 2000× and 5000× magnification, are given in Fig. 14. When these images are examined, it is seen that the density of C-S-H gels has increased visibly compared to 7-day samples and started to cover the structure completely. C-S-

H gels developed in web-like form, completely filling the voids. The web-like structure bonded and developed, reaching approximately 15 μm in size.

SEM images of the samples at 2000× and 5000× magnification at 90 days with a 5% fly ash replacement ratio are given in Fig. 15. When the images were examined, it was observed that the size of the C-S-H gels increased, and the web-like structure thickened and filled the voids. It was observed that the sizes of the C-S-H gels were in the range from 20 to 30 μm. He also observed ettringite needles of range from 20 to 30 μm in size.

SEM images at 7-day samples with 20% fly ash replacement ratio, at 2000× and 5000× magnification, are given in Fig. 16. When the images are examined, it is seen that the web-like structure of the C-S-H gels started to form. CH gels were also observed in the microstructure and it was observed that C-S-H gels started to cover the CH gels with a web-like structure. It was observed that the C-S-H gels that started to fill the gaps reached a size of approximately 10 μm and the CH gels were approximately 20 μm in size.

SEM images of the samples with the same replacement ratio at 2000× and 5000× magnification at 28 days are given in Fig. 17. When these images are examined, it is seen that the density of C-S-H gels has increased visibly compared to 7-day samples and started to cover the structure completely. C-S-H gels developed in web-like form, completely filling the voids. The web-like structure bonded together and developed and reached the size of approximately 20 μm.

SEM images of the samples at 2000× and 5000× magnification at 90 days with a 20% fly ash replacement ratio are given in Fig. 18. When the images were examined, it was observed that the size of the C-S-H gels increased, and the web-like structure thickened and filled the voids. It was observed that the dimensions of the web formed by C-S-H gels were approximately 30 μm.

3.2.4. Microstructure analysis of samples having BA.

Microstructure studies were carried out at 7-, 28- and 90-days curing times according to the 5% and 20% replacement ratio of the bottom ash- substituting samples. SEM images at 7-day samples, with a 5% bottom ash replacement ratio at 2000× and 5000× magnification, are given in Fig. 19. When the images are examined, it is seen that the web-like structure of the C-S-H gels started to form. It was observed that the sizes of the C-S-H gels that started to fill the gaps were in the range of approximately 5 μm.

SEM images of the samples with the same replacement ratio at 2000× and 5000× magnification at 28 days are given in Fig. 20. When these images are examined, it is seen that the density of C-S-H gels has increased visibly compared to 7-day samples and started to cover the structure completely. C-S-H gels developed in web-like form, completely filling the voids. The web-like structure bonded together and developed and reached the size of approximately 10 μm.

SEM images obtained at 2000× and 5000× magnification at 90-day samples with a 5% bottom ash replacement ratio are given in Fig. 21. When the images were examined, it was observed that the size of

the C-S-H gels increased compared to the 7- and 28-day samples with the same replacement ratio and the web-like structure became denser. It was observed that the dimensions of the web formed by C-S-H gels were in the range of approximately ranges from 20 to 30 μm.

SEM images at 7-day samples with a 20% replacement ratio, taken at 2000× and 5000× magnification, are given in Fig. 22. When the images were examined, it was observed that the web-like structure of C-S-H gels started to form. CH gels were also seen in the microstructure, and it was observed that the web-like structure of C-S-H gels developed around the CH gels. It was observed that the C-S-H gels that started to fill the gaps reached a size of approximately 5 μm and that the CH gels were in the range of approximately ranges from 5 to 10 μm.

SEM images of the samples with the same replacement ratio at 2000× and 5000× magnification at 28 days are given in Fig. 23. When these images are examined, it is seen that the density of C-S-H gels increased at 7-day-old samples and started to cover the structure completely. It is seen that the cactus-shaped structures formed by the combination of C-S-H gels reach approximately 20 μm in size.

SEM images obtained at 2000× and 5000× magnification at 90-day samples with 20% bottom ash replacement ratio are given in Fig. 24. When the images were examined, it was observed that the sizes of the C-S-H gels increased compared to the 7- and 28-day old samples with the same replacement ratio, the web-like structure was thickened by intertwining and took the form of a cactus. It was observed that the dimensions of the web-like formed by the C-S-H gels were in the range of approximately ranges from 20 to 30 μm.

According to the microstructural analysis by the scanning electron microscope, it was found more C-S-H concentration and bigger C-S-H gels in cement mortar composites incorporating blast furnace slag. Recall that the calcium oxide (CaO) and SiO_2 amounts of slag are 39.60% and 36.10, respectively. The high amount of calcium oxide (CaO) could contribute to the formation of C_3S and C_2S and thus C-S-H forming with the pozzolanic capability and the filler effect might result in high compactness through mechanical particle filling and further formation of calcium-silicate-hydrate (C-S-H) gels by using GGBS. Note that the highest loss on ignition is 5.21, which is in bottom ash, so the shortest C-S-H gels are found in cement mortar composites incorporating bottom ash. It seems that filler effect and pozzolanic capability resulted in high compactness through mechanical particle filling and further formation of calcium-silicate-hydrate (C-S-H) gels. These results were found to be consistent with compressive strength results.

4. Conclusion

This study investigated the effect of the microstructural and mechanical properties of cement mortar composites incorporating fly ash, slag, and bottom ash as supplementary cementitious materials with similar Blaine fineness. The fly ash, slag, and bottom ash were ground at a similar cement Blaine fineness (~ 3300 cm^2/g) and then by replacing 5% and 20% with cement, the 7-, 28-, 90-day microstructural and

compressive strength properties of cement mortar composites incorporating SCMs were examined. Following findings were drawn:

- It is considered that the differences in the compressive strength and microstructure of cement mortar composites incorporating slag, fly ash, and bottom ash with similar Blaine fineness caused by the differences in the chemical composition of the samples. Although the material with the highest amount of SiO_2 is fly ash, due to the low amount of calcium oxide (CaO), C_3S could not contribute as much to the formation of C_2S as slag. Therefore, the compressive strength of the cement mortar composites incorporating slag was found to be higher than the fly ash and bottom ash substituting samples.
- As a result of the microstructure analysis of the produced cement mortar samples, it was observed that the web-like structure of C-S-H gels became denser and filled the voids in the microstructure depending on the maturation period.
- Microstructure analyses showed the reduced quantity of voids in the cement mortar composites incorporating SCMs, due to C-S-H phase formation.
- When the mechanical strength and microstructural properties were evaluated, it was seen that the strength and microstructural properties improved in proportion to the development of C-S-H gels.

As a result, it is likely to improve the mechanical and microstructural properties of the cement mortar composites using more slag replacement ratio according to other SCMs. This will decrease the required amount of cement for target properties by using SCMs type. Depending on the lessen in the quantity of cement, the number of CO_2 emitted to nature will also decrease. These supplementary cementitious materials could be used in the construction sector and could much advantage the economy and environment.

Declarations

Acknowledgments

We thank the anonymous referees for their useful suggestions.

Author Contributions

Ozer Sevim: Investigation, Methodology, Conceptualization, Writing-review and editing, Supervision.

Cagri Goktug Sengul: Methodology, Investigation, Visualization, Writing- original draft.

Funding

The authors of the manuscript did not receive any funding, grants, or in-kind support in support of the research or the preparation of the manuscript.

Data Availability

There is no any other data and material associated with this manuscript

Ethics declarations

Conflict of Interest

The authors declare that they have no conflict of interest.

Consent to Participate

The authors give full consent to participate in this research work.

Consent for Publication

The authors give full consent for publication of this research work.

References

1. Lothenbach B, Scrivener K, Hooton RD (2011) Supplementary cementitious materials. Cem Concr Res 41(12):1244–1256.
2. Juenger MC, Siddique R (2015) Recent advances in understanding the role of supplementary cementitious materials in concrete. Cem Concr Res 78:71–80.
3. Aprianti E, Shafigh P, Bahri S, Farahani JN (2015) Supplementary cementitious materials origin from agricultural wastes–A review. Constr Build Mater 74:176–187.
4. Johari MM, Brooks JJ, Kabir S, Rivard P (2011) Influence of supplementary cementitious materials on engineering properties of high strength concrete. Constr Build Mater 25(5):2639–2648.
5. Sahmaran M, Yildirim G, Erdem TK (2013). Self-healing capability of cementitious composites incorporating different supplementary cementitious materials. Cem Concr Compos 35(1):89–101.
6. Snellings R, Mertens G, Elsen J (2012) Supplementary cementitious materials. Rev Mineral Geochem 74(1):211–278.
7. Mehta PK (2005) Concrete: Structure, properties and materials. Prentice Hall, New York, USA.
8. Neville AM (1981) Properties of Concrete. Longman Scientific and Technical, New York.
9. Meyer C (2009) The greening of the concrete industry. Cem Concr Compos 31(8):601–605.
10. Ural B, Turanli L, Mehta PK (2007) High-volume natural pozzolan concrete for structural applications. ACI Mater J 104(5):535–538.
11. Madlool NA (2011) A critical review on energy use and savings in the cement industries. Renewable Sustainable Energy Rev 15(4):2042–2060.
12. ASTM C618-19 (2019) Standard specification for coal fly ash and raw or calcined natural pozzolan for use in concrete. ASTM International, West Conshohocken, PA.

13. Sabir BB, Wild S, Bai J (2001) Metakaolin and calcined clays as pozzolans for concrete: a review. Cem Concr Compos 23(6):441–454.
14. Aruntas HY (2006) The potential of fly ash usage in construction sector. J Fac Eng Arch Gazi Univ 21(1):193-203 (in Turkish).
15. Rodrıguez-Camacho RE, Uribe-Afif R (2002) Importance of using the natural pozzolans on concrete durability. Cem Concr Res 32(12):1851–1858.
16. Massazza F (1993) Pozzolanic cements. Cem Concr Compos15(4):185–214.
17. Moropoulou A, Bakolas A, Aggelakopoulou E (2004) Evaluation of pozzolanic activity of natural and artificial pozzolans by thermal analysis. Thermochim Acta 420(1-2):135–140.
18. Murthi P, Poongodi K, Awoyera PO, Gobinath R, Saravanan R (2020) Enhancing the Strength Properties of High-Performance Concrete Using Ternary Blended Cement: OPC, Nano-Silica, Bagasse Ash. Silicon 12:1949–1956.
19. Toklu K, Şimşek O, Aruntaş HY (2019) Investigation of the usability of high-performance fiber-reinforced cement composites containing high-volume fly ash and nanomaterials as repair mortar. J Aust Ceram Soc 55:789–797.
20. Rashad AM, Sadek DM (2019). Influence of Different Particle Sizes of Blast-Furnace Slag as a Fine Aggregate on Mechanical Strength and Abrasion Resistance of Concrete. Silicon 12:2365–2373.
21. Toklu K, Şimşek O (2018). Investigation of mechanical properties of repair mortars containing high-volume fly ash and nano materials. J Aust Ceram Soc 54(2):261–270.
22. Toklu K (2021) Investigation of Mechanical and Durability Behaviour of High Strength Cementitious Composites Containing Natural Zeolite and Blast-furnace Slag. Silicon.
23. Demir İ, Güzelkücük S, Sevim Ö (2018) Effects of sulfate on cement mortar with hybrid pozzolan substitution. Eng Sci Tech Int J 21(3):275–283.
24. Guzelkucuk S, Demir I, Sevim O, Kalkan I (2020) Mechanical properties and microstructure of cement multicomponent systems containing pozzolan materials under sulfate attack. Cem Wapno Beton 25(2):137–153.
25. Sata V, Jaturapitakkul C, Kiattikomol K (2007) Influence of pozzolan from various by-product materials on mechanical properties of high-strength concrete. Constr Build Mater 21(7):1589–1598.
26. Ghrici M, Kenai S, Said-Mansour M (2007) Mechanical properties and durability of mortar and concrete containing natural pozzolana and limestone blended cements. Cem Concr Compos 29(7):542–549.
27. Bentz DP, Hansen AS, Guynn JM (2011) Optimization of cement and fly ash particle sizes to produce sustainable concretes. Cem Concr Compos 33(8):824–831.
28. Bentz DP, Ferraris CF, Filliben JJ (2011) Optimization of particle sizes in high volume fly ash blended cements. US Department of Commerce, National Institute of Standards and Technology.
29. Slanička S (1991) The influence of fly ash fineness on the strength of concrete. Cem Concr Res 21(2-3):285–296.

30. Zhang X, Wu K, Yan A (2004) Carbonation property of hardened binder pastes containing super-pulverized blast-furnace slag. Cem Concr Compos 26(4):371–374.
31. Li G, Zhao X (2003) Properties of concrete incorporating fly ash and ground granulated blast-furnace slag. Cem Concr Compos 25(3):293–299.
32. Monzo J, Paya J, Peris-Mora E (1994) A preliminary study of fly ash granulometric influence on mortar strength. Cem Concr Res 24(4):791–796.
33. Sevim Ö, Demir İ (2019) Physical and permeability properties of cementitious mortars having fly ash with optimized particle size distribution. Cem Concr Compos 96: 266–273.
34. Sevim Ö, Demir İ (2019) Optimization of fly ash particle size distribution for cementitious systems with high compactness. Constr Build Mater 195:104–114.
35. Filazi A, Demir I, Sevim O (2020) Enhancement on mechanical and durability performances of binary cementitious systems by optimizing particle size distribution of fly ash. Archiv Civ Mech Eng 20(2):58.
36. Karim MR, Hossain MM, Elahi MMA, Zain MFM (2020) Effects of source materials, fineness and curing methods on the strength development of alkali-activated binder. J Build Eng 29: 101147.
37. Ma Z, Tang Q, Wu H, Xu J, Liang C (2020) Mechanical properties and water absorption of cement composites with various fineness and contents of waste brick powder from C&D waste. Cem Concr Compos 114: 103758.
38. Alaskar A, Hooton RD (2020) Effect of binder fineness and composition on length change of high-performance concrete. Constr Build Mater 237:117537.
39. Ahmed Shaikh FU, Arel HŞ (2020) Effects of curing types, fly ash fineness and fibre lengths on mechanical and impact properties of steel fibre reinforced concretes. Aust J Civ Eng 18(2):231–245.
40. Sun Y, Wang KQ, Lee HS (2021) Prediction of compressive strength development for blended cement mortar considering fly ash fineness and replacement ratio. Constr Build Mater 271:121532.
41. De Maeijer PK, Craeye B, Snellings R, Kazemi-Kamyab H, Loots M, Janssens K, Nuyts G (2020) Effect of ultra-fine fly ash on concrete performance and durability. Constr Build Mater 263:120493.
42. Hallet V, De Belie N, Pontikes Y (2020) The impact of slag fineness on the reactivity of blended cements with high-volume non-ferrous metallurgy slag. Constr Build Mater 257:119400.
43. Khongpermgoson P, Boonlao K, Ananthanet N, Thitithananon T, Jaturapitakkul C, Tangchirapat W, Ban CC (2020) The mechanical properties and heat development behavior of high strength concrete containing high fineness coal bottom ash as a pozzolanic binder. Constr Build Mater 253:119239.
44. TS EN 197-1 (2012) Cement–Part 1: Composition, specifications and conformity criteria for common cements. Turkish Standard Institution, Ankara (in Turkish).
45. TS EN 196-1 (2016) Methods of testing cement–Part 1: Determination of strength. Turkish Standard Institution, Ankara.
46. Ramanathan S, Moon H, Croly M, Chung CW, Suraneni P (2019) Predicting the degree of reaction of supplementary cementitious materials in cementitious pastes using a pozzolanic test. Constr Build

Mater 204:621–630.
47. ASTM C311 / C311M-18 (2018) Standard Test Methods for Sampling and Testing Fly Ash or Natural Pozzolans for Use in Portland-Cement Concrete. ASTM International, West Conshohocken, PA.
48. Labbaci Y, Abdelaziz Y, Mekkaoui A, Alouani A, Labbaci B (2017) The use of the volcanic powders as supplementary cementitious materials for environmental-friendly durable concrete. Constr Build Mater 133:468–481.
49. Dembovska L, Bajare D, Pundiene I, Vitola L (2017). Effect of pozzolanic additives on the strength development of high performance concrete. Procedia Eng 172:202–210.
50. Papadakis VG (2000). Effect of fly ash on Portland cement systems: Part II. High-calcium fly ash. Cem Concr Res 30(10):1647–1654.
51. Chindaprasirt P, Chareerat T, Sirivivatnanon V (2007). Workability and strength of coarse high calcium fly ash geopolymer. Cem Concr Compos 29(3):224–229.

Figures

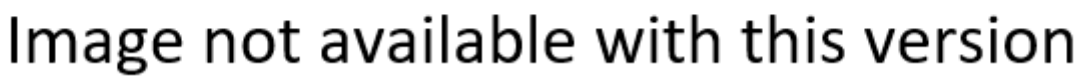

Figure 1

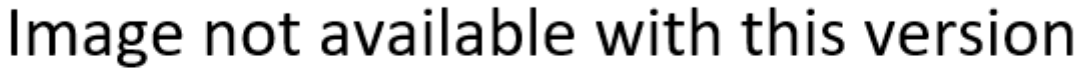

Figure 2

Image not available with this version

Figure 3

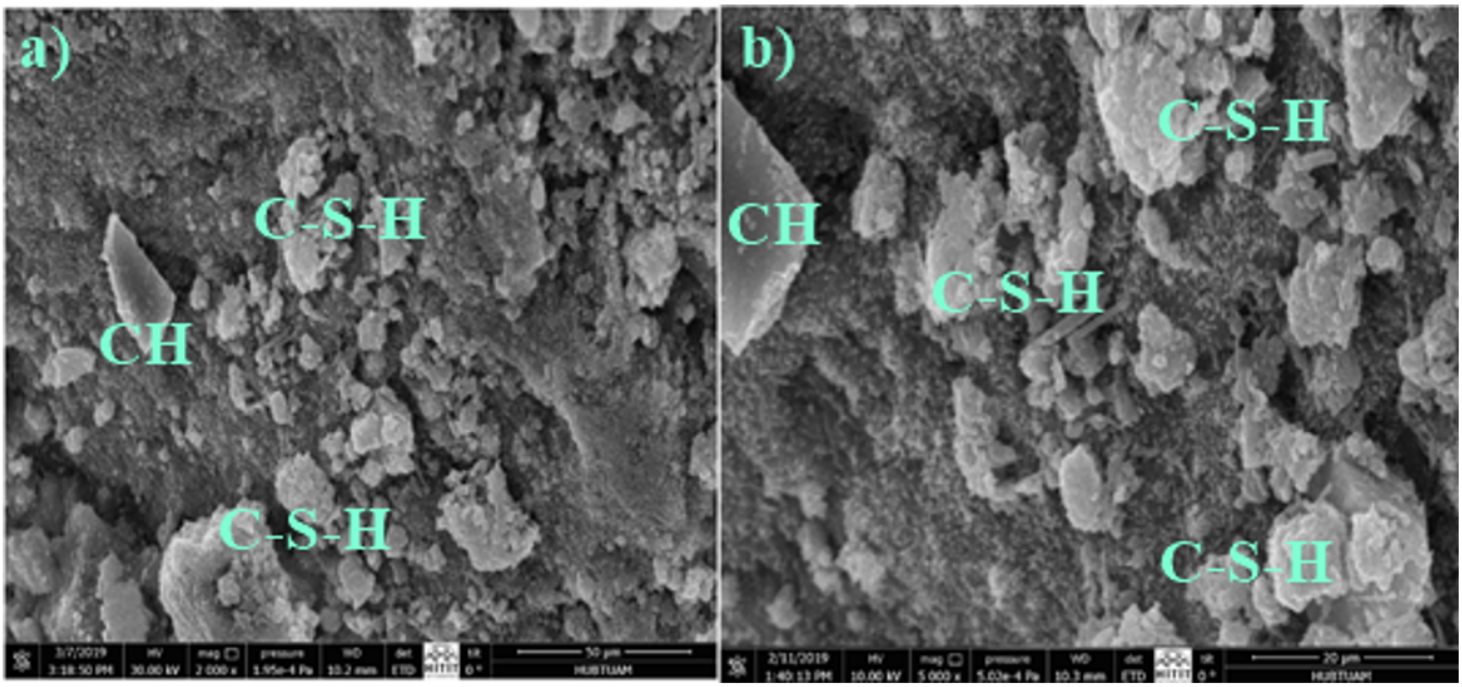

Figure 4

SEM images of additive-free samples at (a) 2000× (b) 5000× magnification for 7-days.

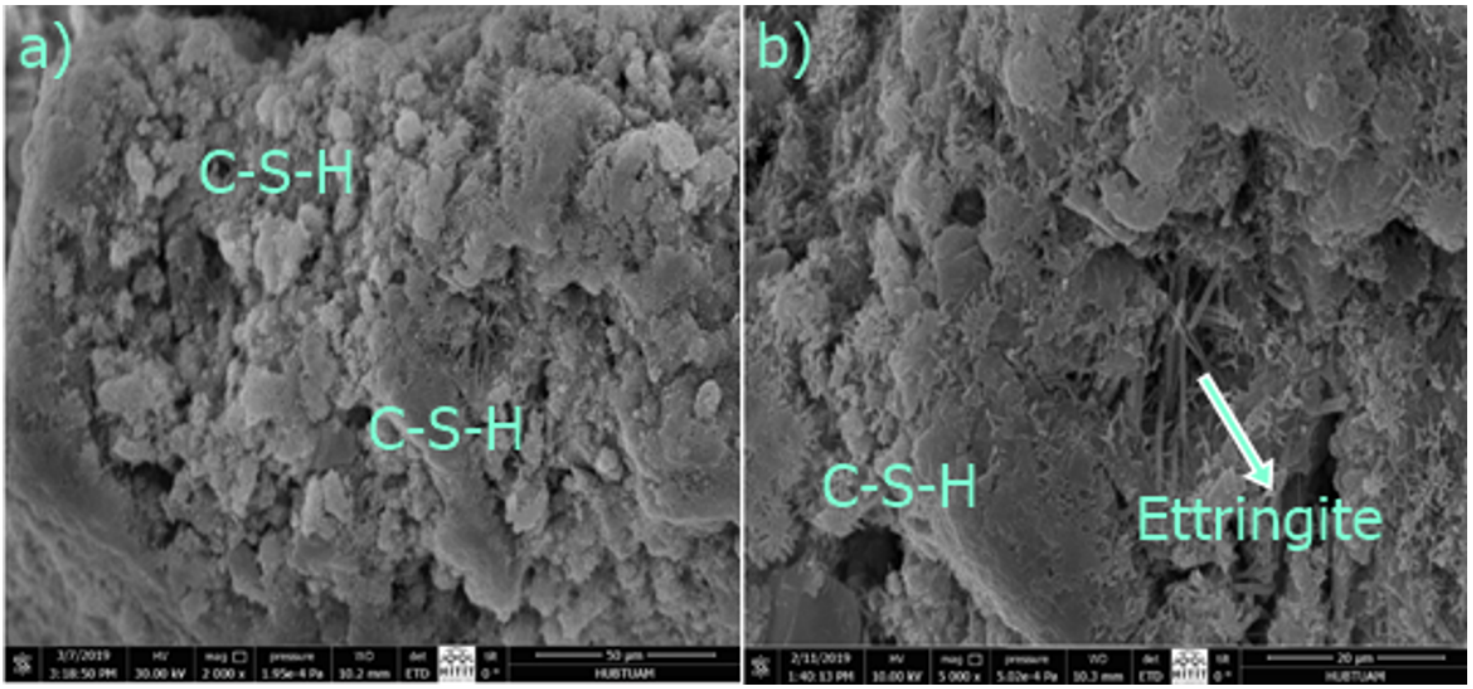

Figure 5

SEM images of additive-free samples at (a) 2000× (b) 5000× magnification at 28-days.

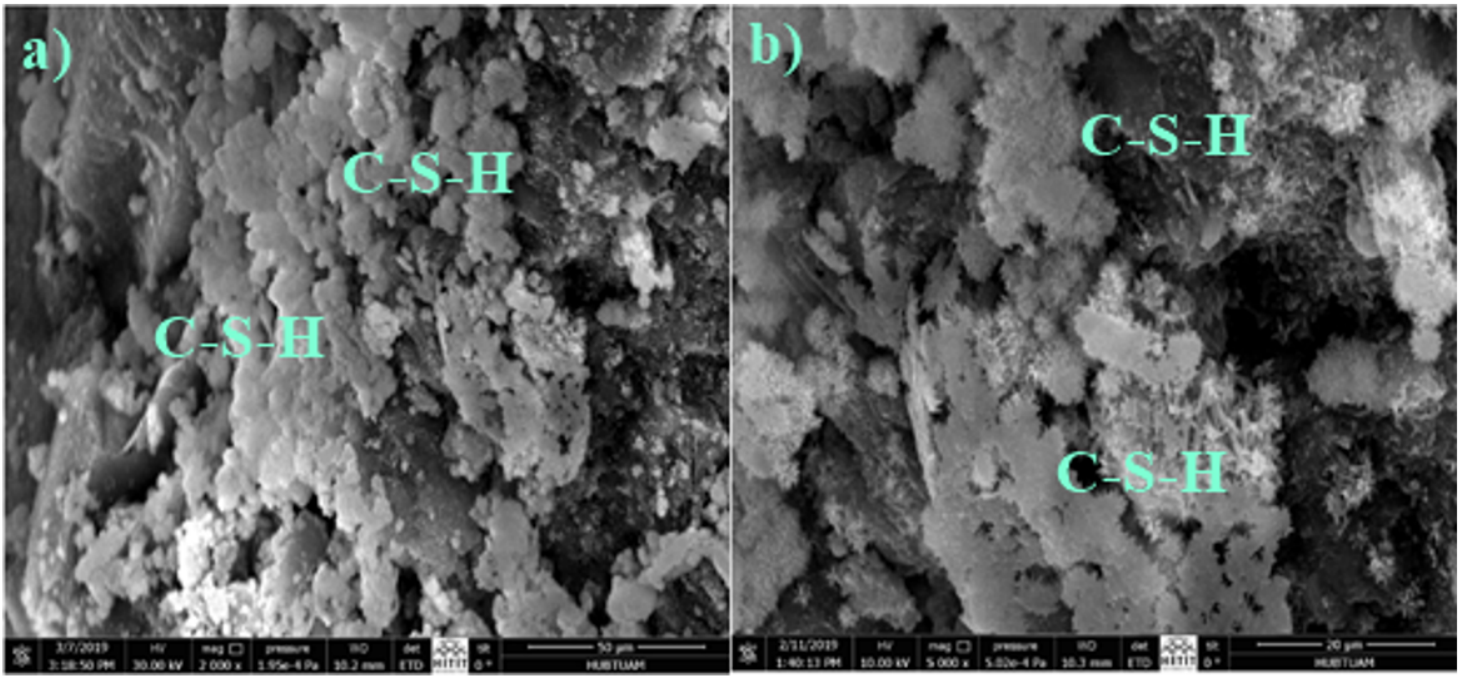

Figure 6

SEM images of additive-free samples at (a) 2000× (b) 5000× magnification at 90-days.

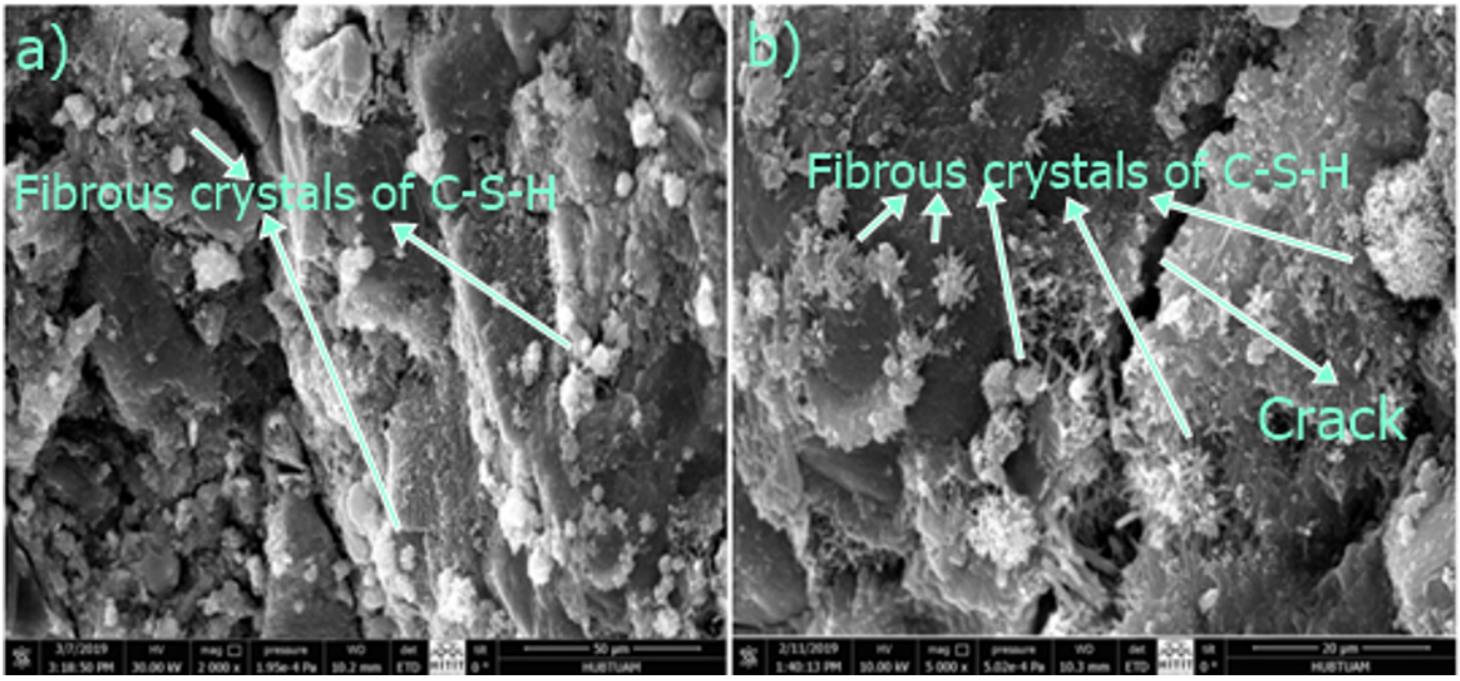

Figure 7

SEM images of samples having 5% GGBFS at (a) 2000× (b) 5000× magnification at 7-days.

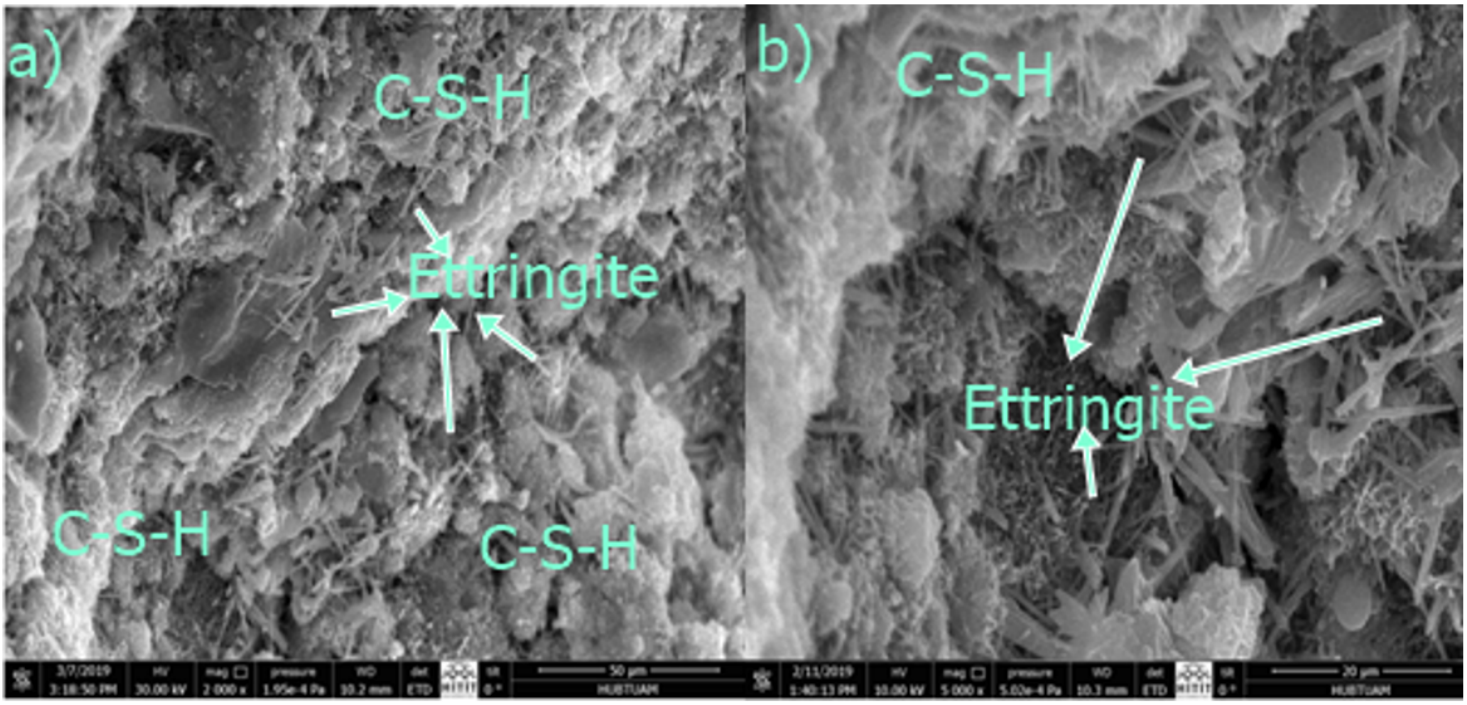

Figure 8

SEM images of samples having 5% GGBFS at (a) 2000× (b) 5000× magnification at 28-days.

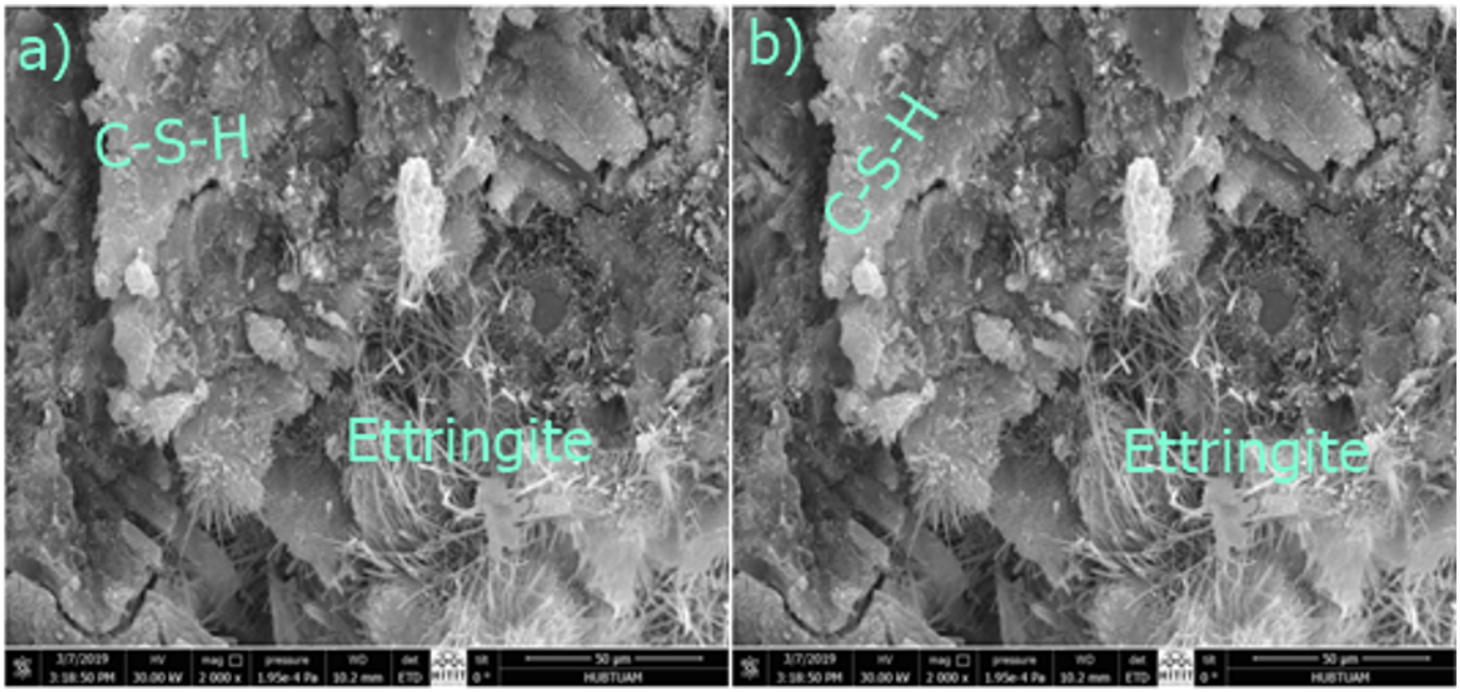

Figure 9

SEM images of samples having 5% GGBFS at (a) 2000× (b) 5000× magnification at 90-days.

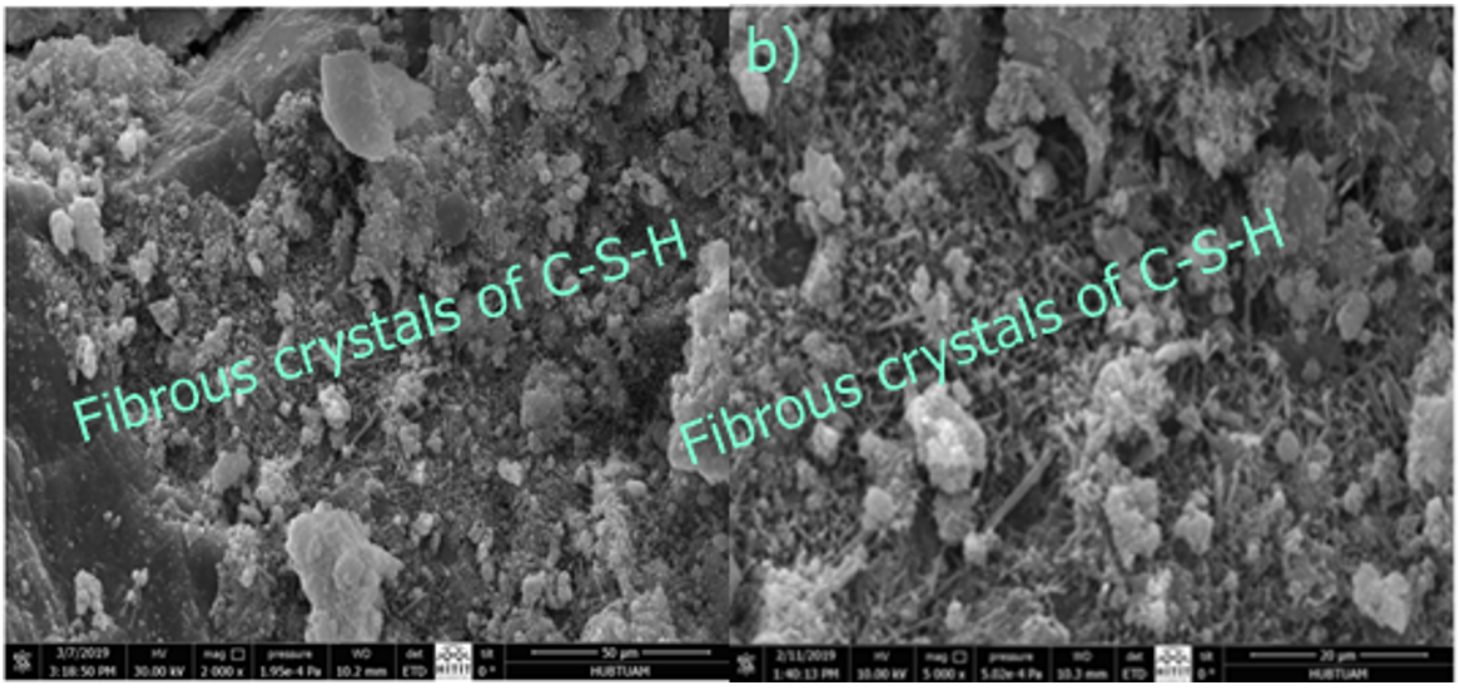

Figure 10

SEM images of samples having 20% GGBFS at (a) 2000× (b) 5000× magnification at 7-days.

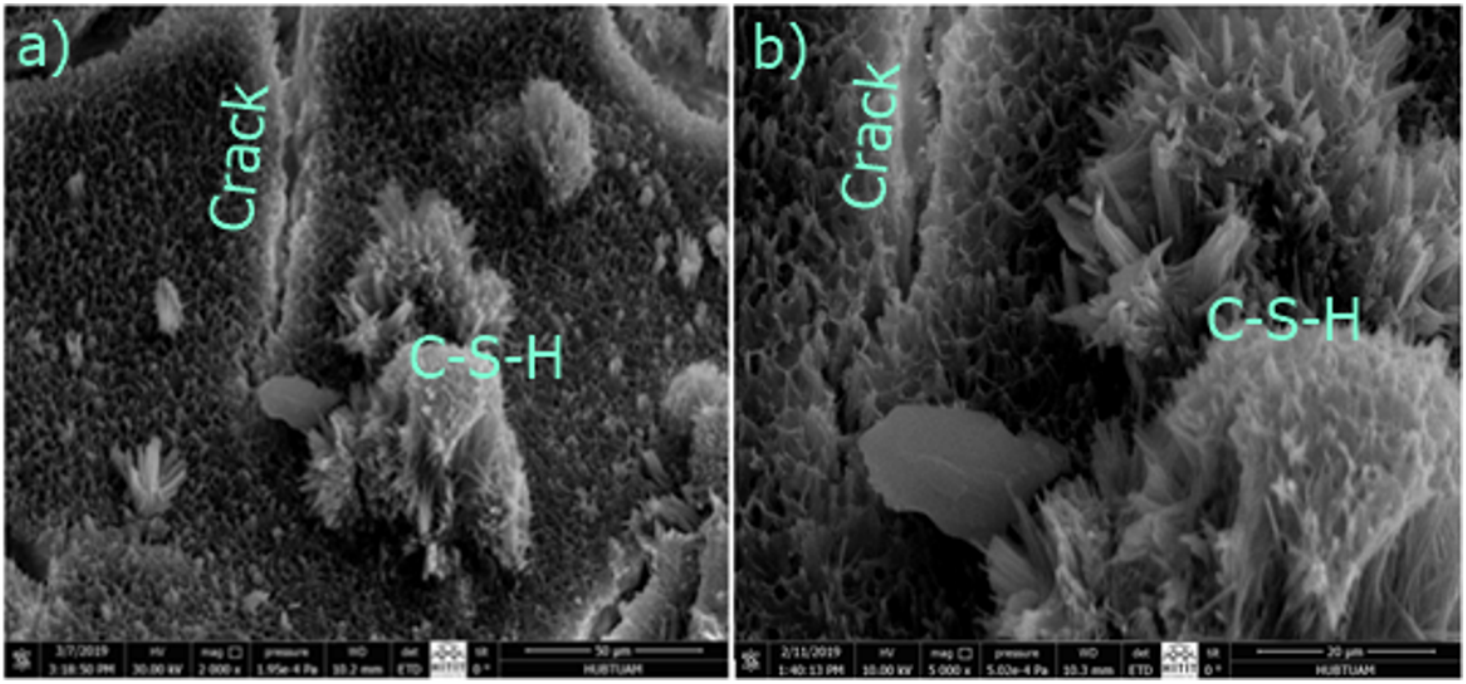

Figure 11

SEM images of samples having 20% GGBFS at (a) 2000× (b) 5000× magnification at 28-days.

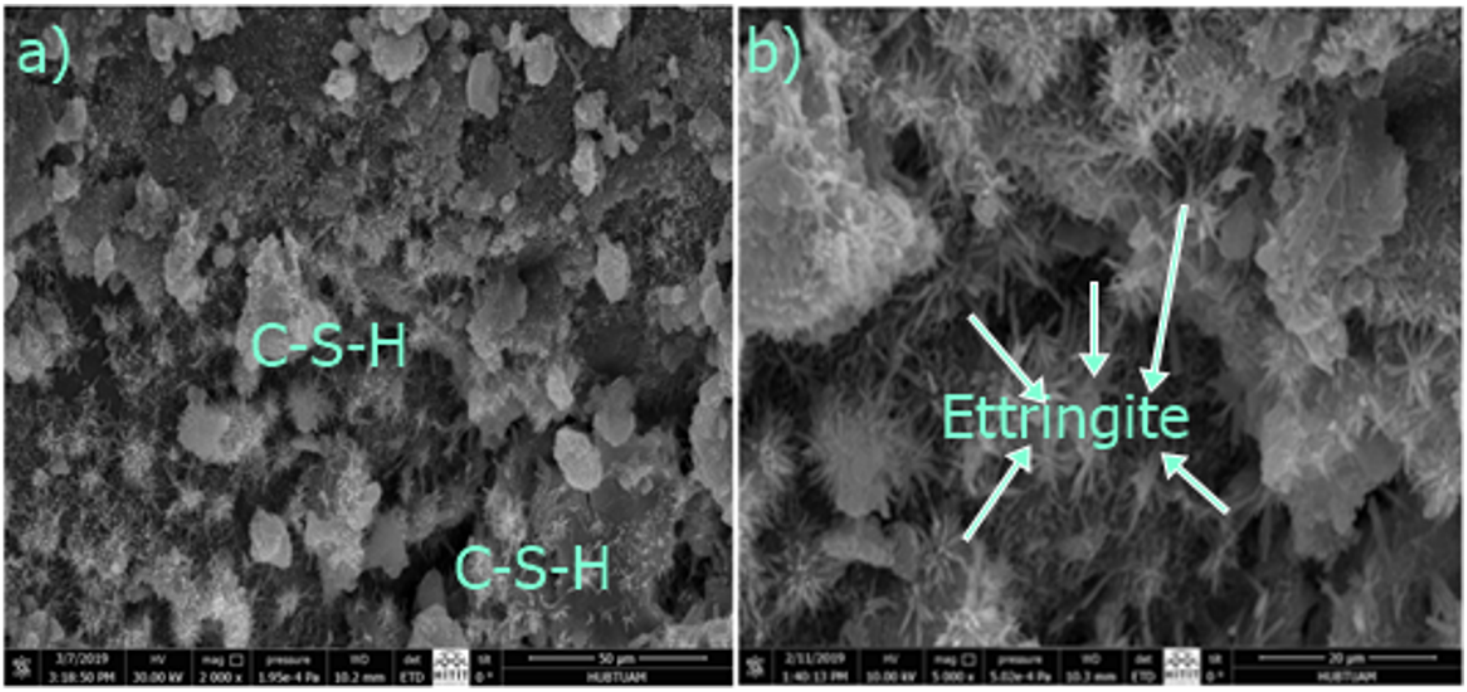

Figure 12

SEM images of samples having 20% GGBFS at (a) 2000× (b) 5000× magnification at 90-days.

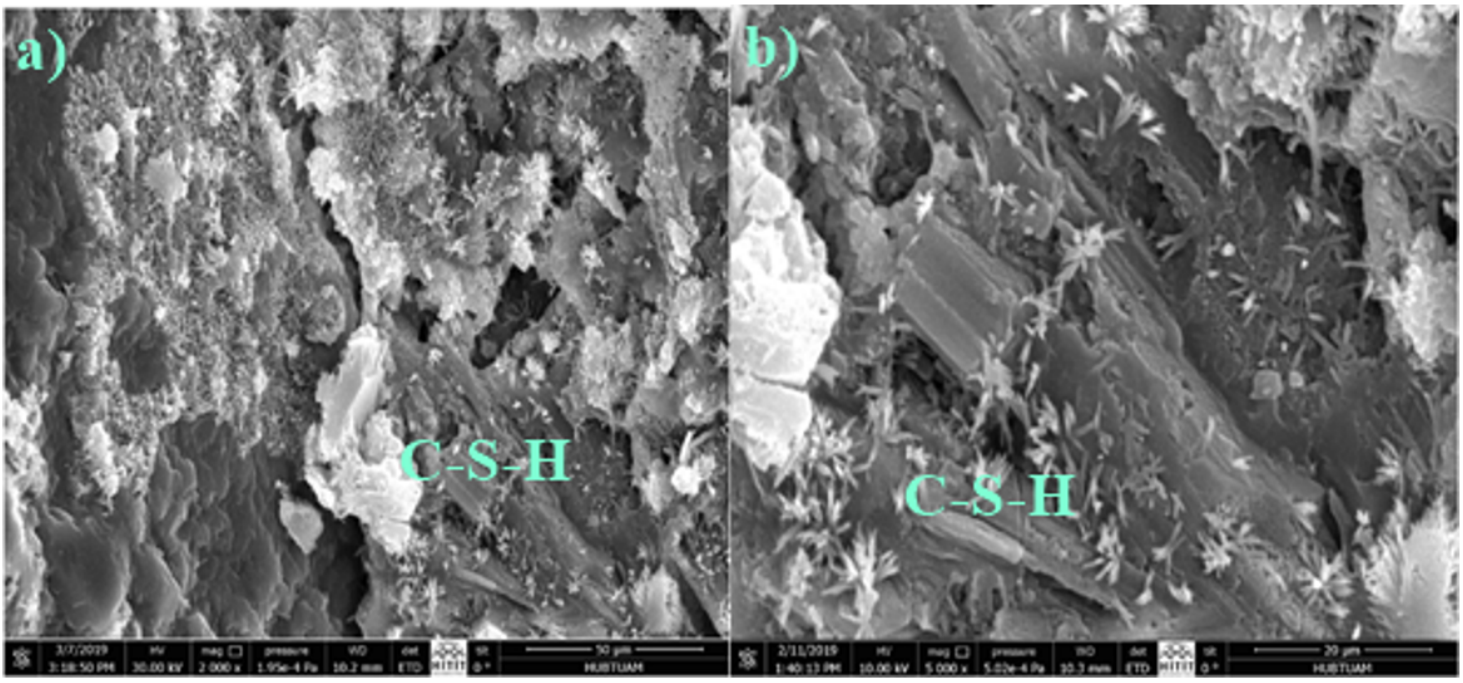

Figure 13

SEM images of samples having 5% FA at (a) 2000× (b) 5000× magnification at 7-days.

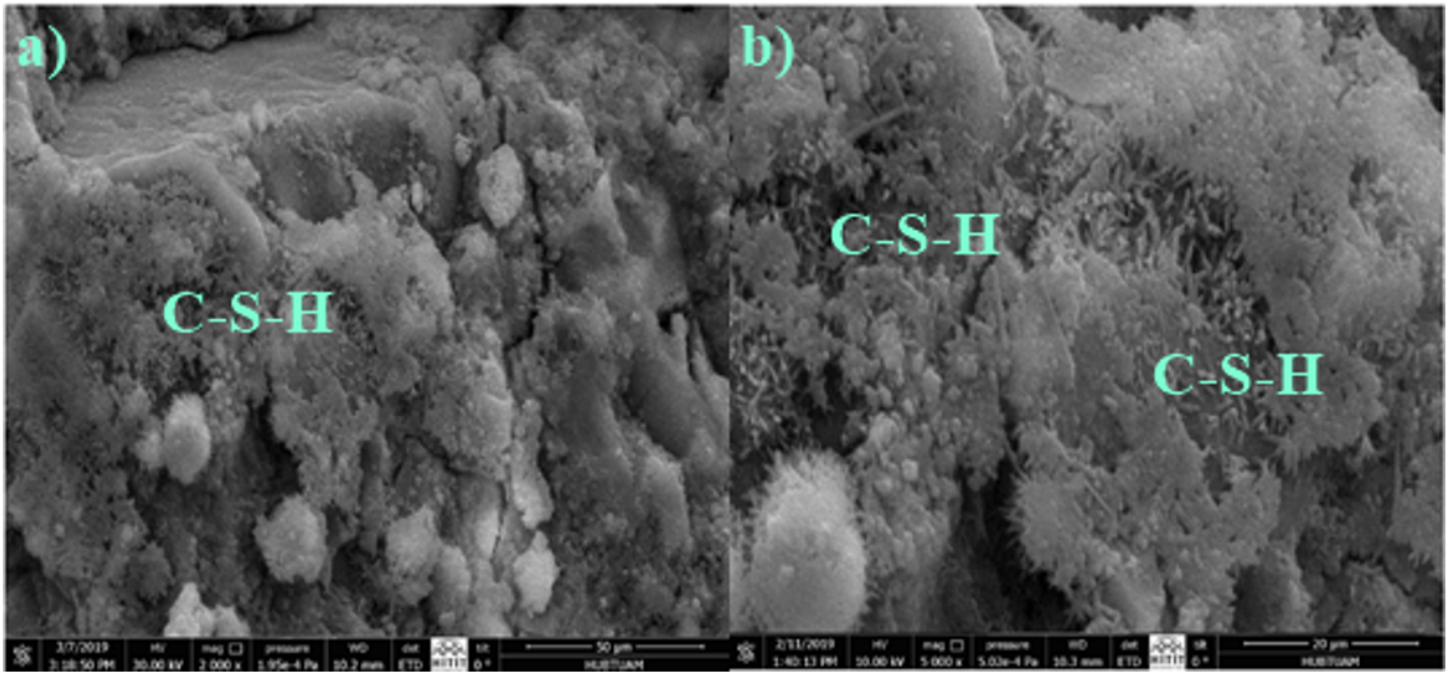

Figure 14

SEM images of samples having 5% FA at (a) 2000× (b) 5000× magnification at 28-days.

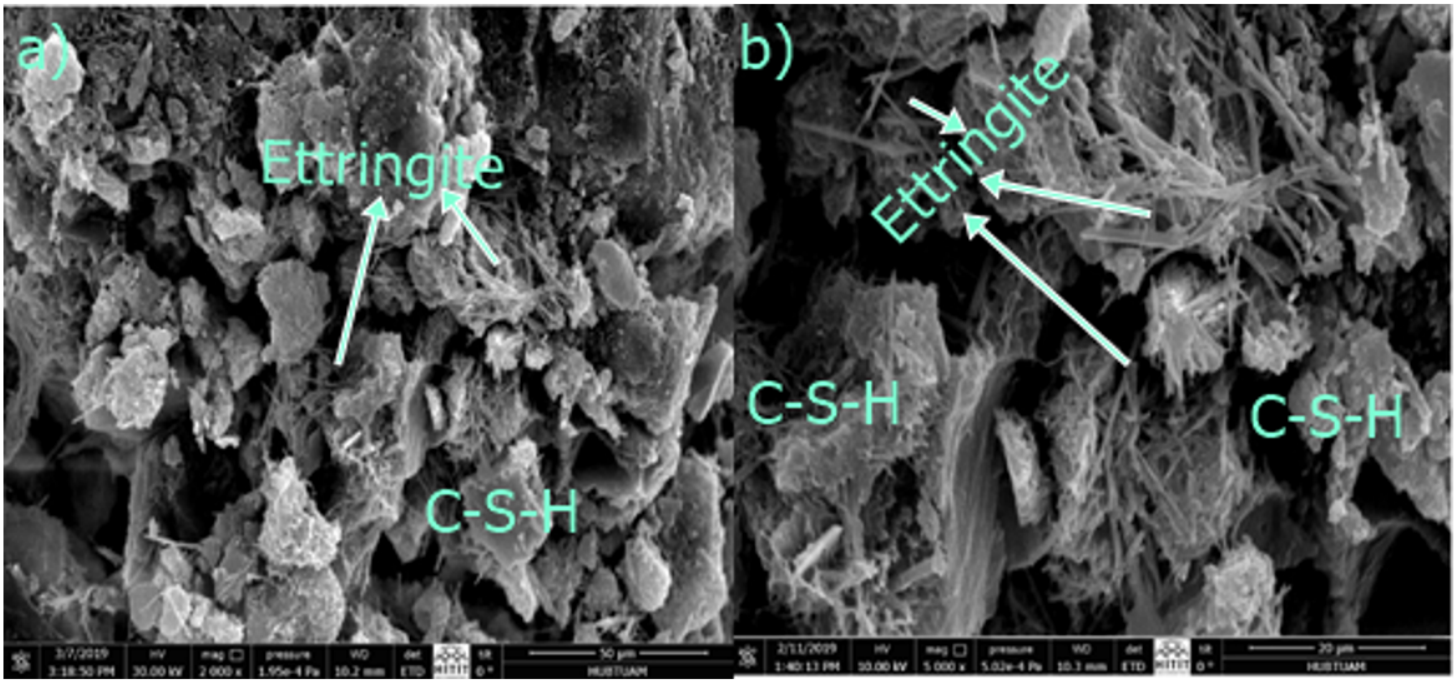

Figure 15

SEM images of samples having 5% FA at (a) 2000× (b) 5000× magnification at 90-days.

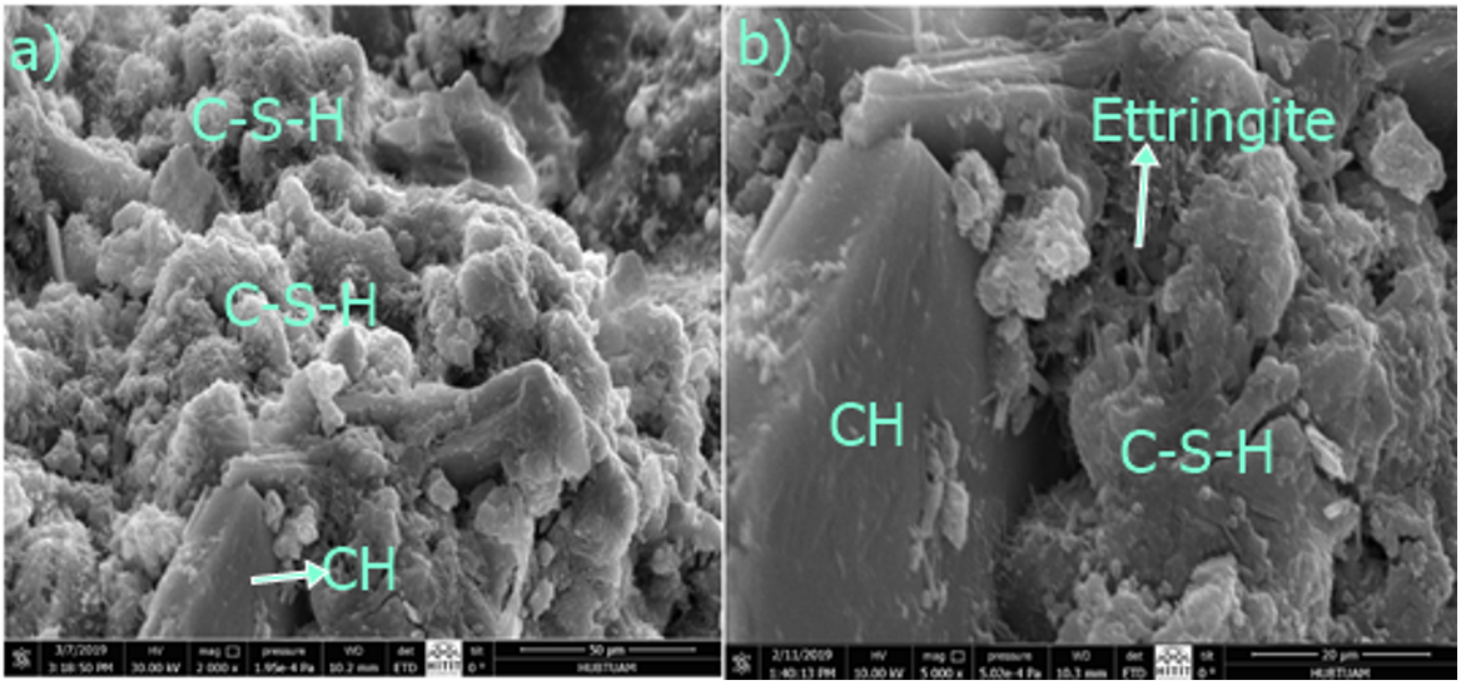

Figure 16

SEM images of samples having 20% FA at (a) 2000× (b) 5000× magnification at 7-days.

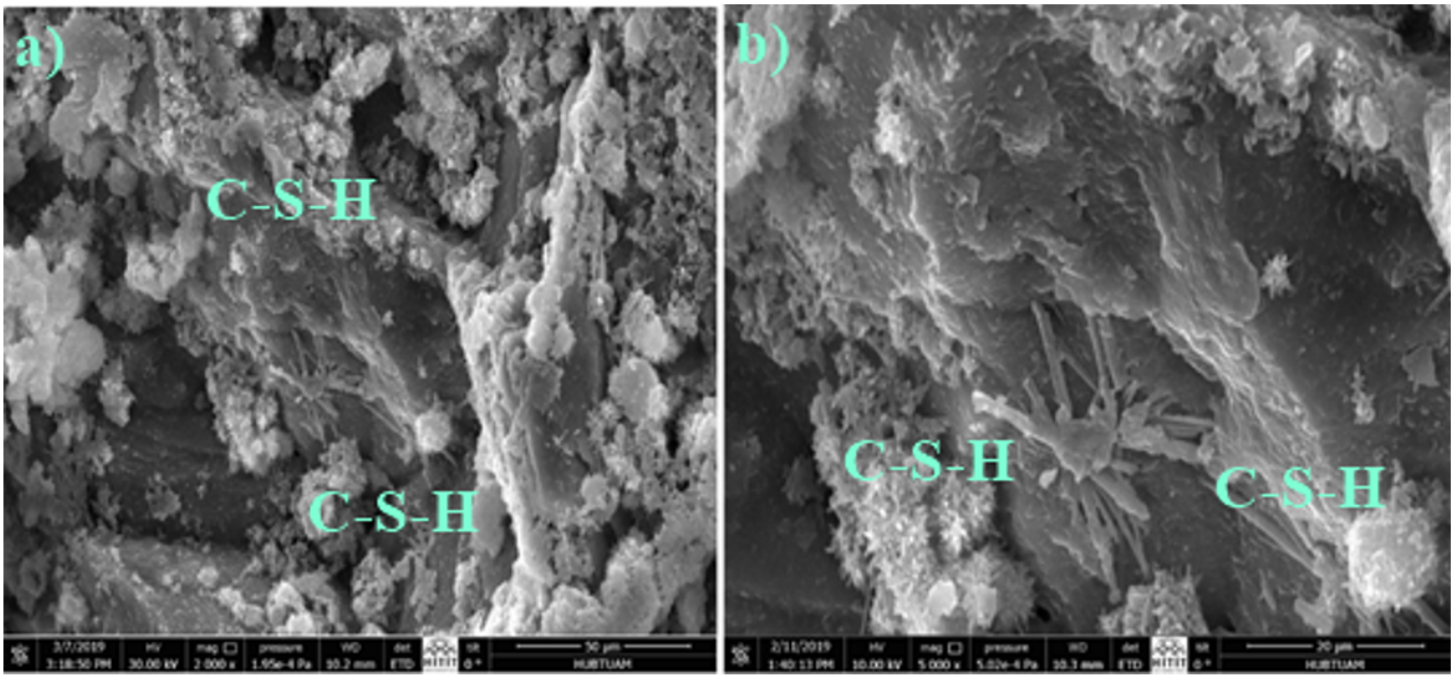

Figure 17

SEM images of samples having 20% FA at (a) 2000× (b) 5000× magnification at 28-days.

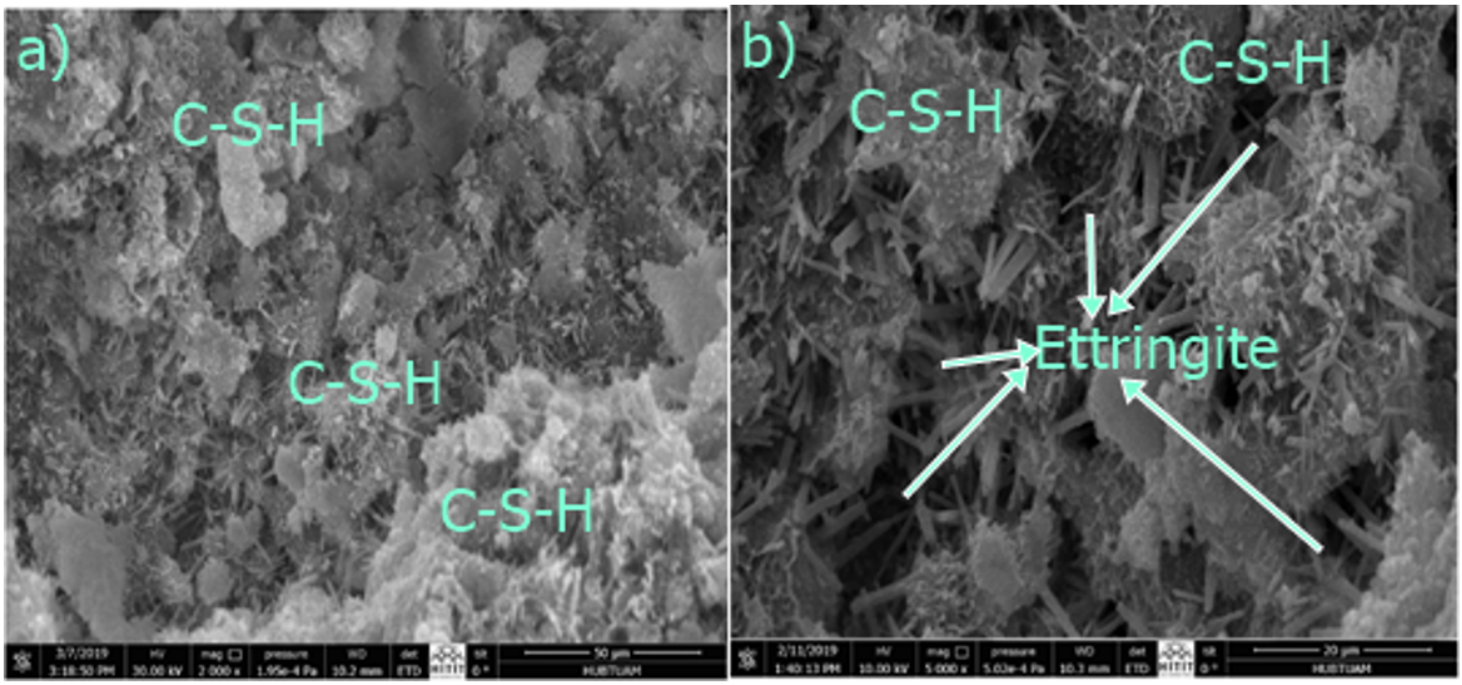

Figure 18

SEM images of samples having 20% FA at (a) 2000× (b) 5000× magnification at 90-days.

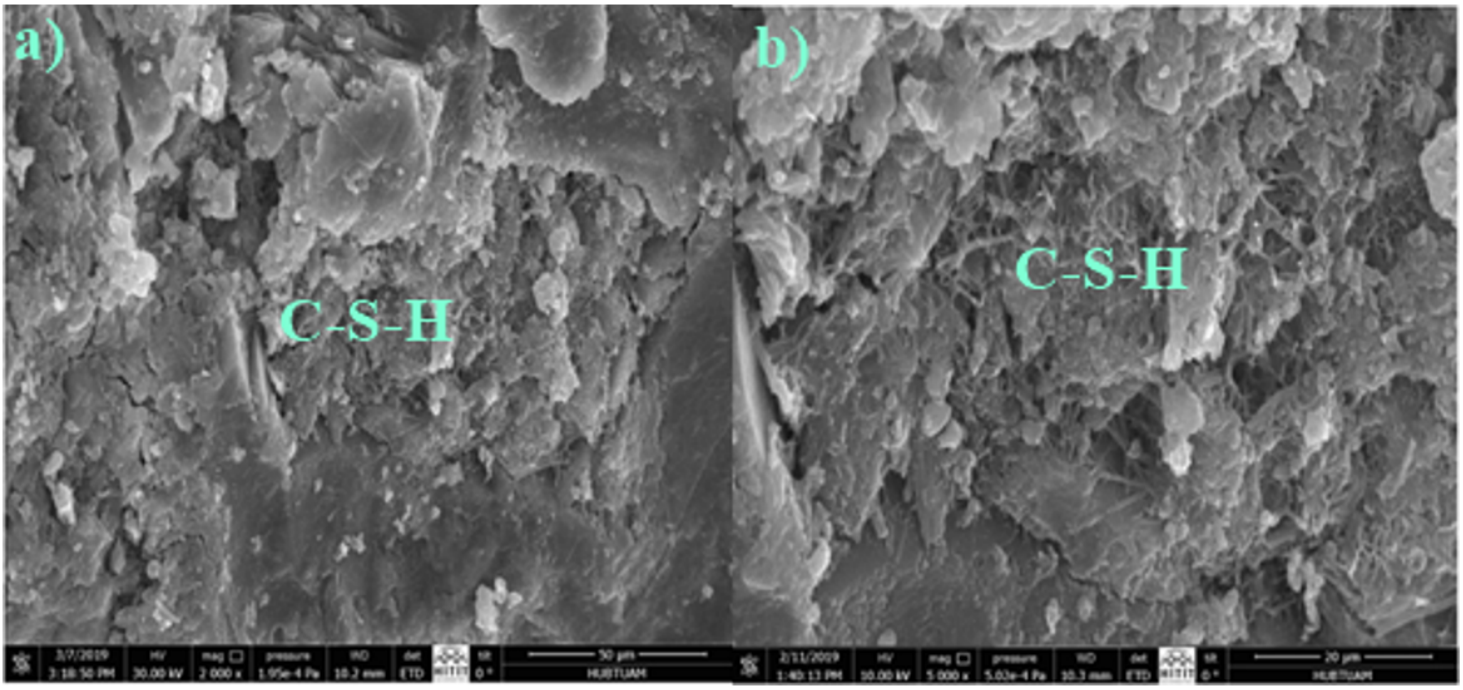

Figure 19

SEM images of samples having 5% BA at (a) 2000× (b) 5000× magnification at 7-days.

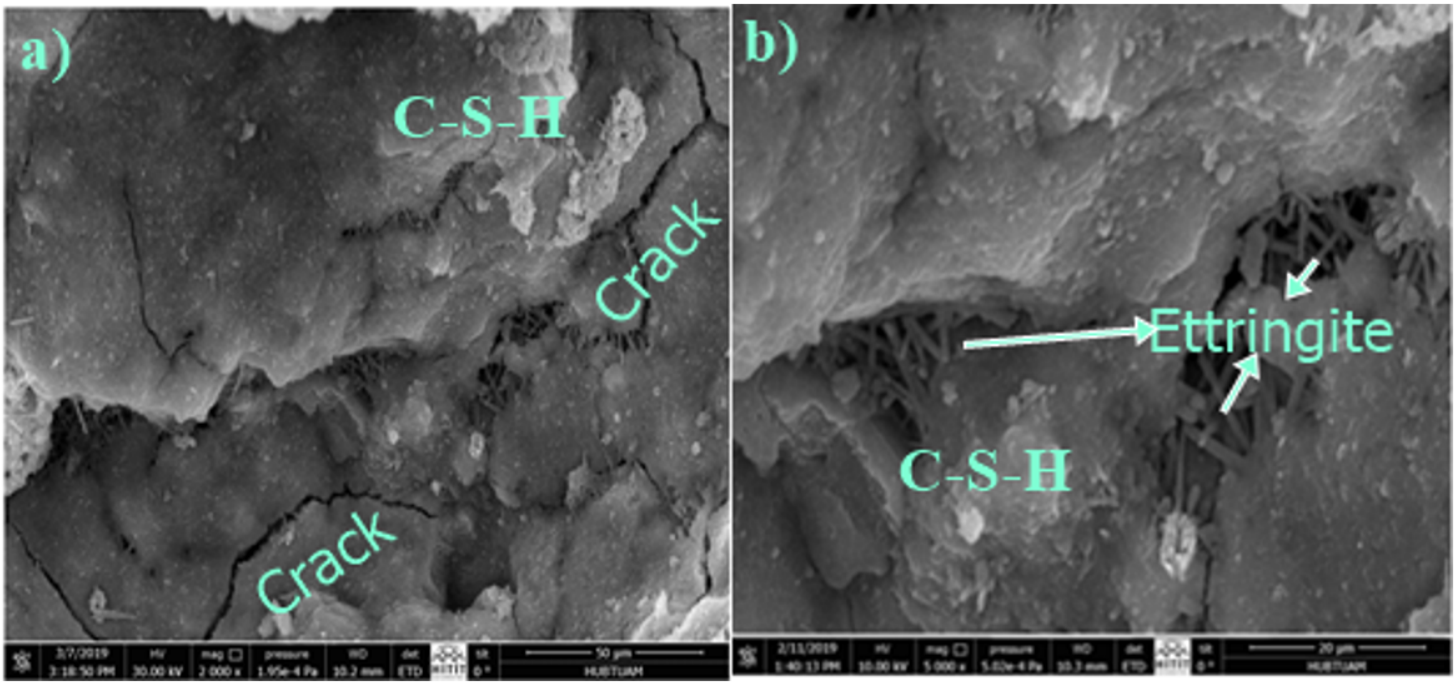

Figure 20

SEM images of samples having 5% BA at (a) 2000× (b) 5000× magnification at 28-days.

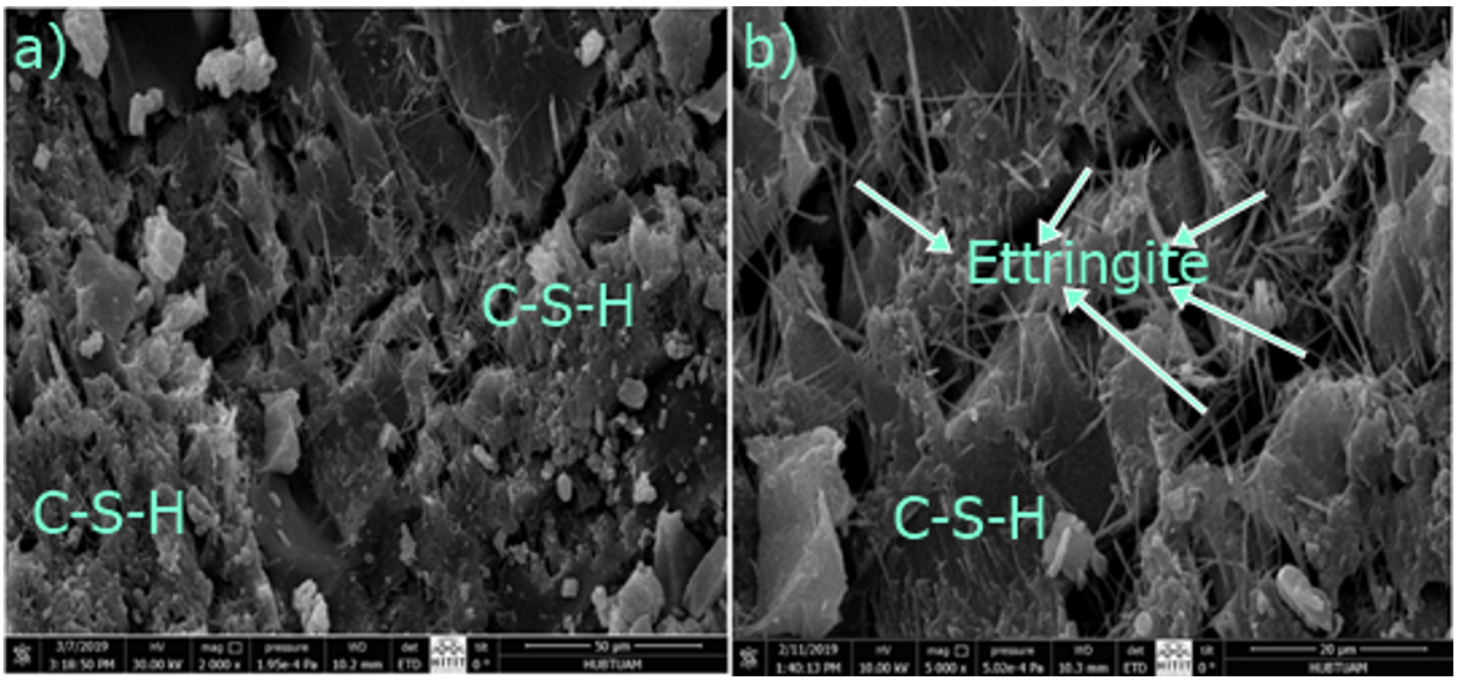

Figure 21

SEM images of samples having 5% BA at (a) 2000× (b) 5000× magnification at 90-days.

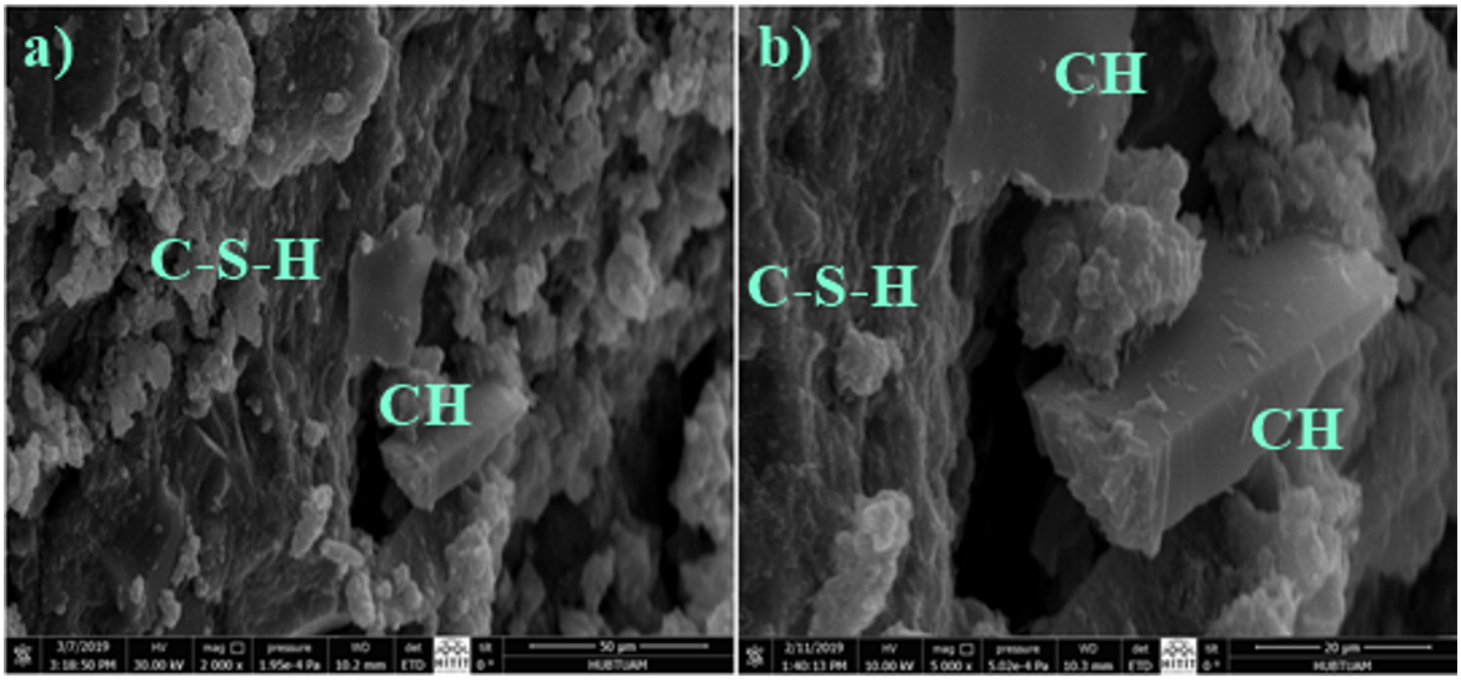

Figure 22

SEM images of samples having 20% BA at (a) 2000× (b) 5000× magnification at 7-days.

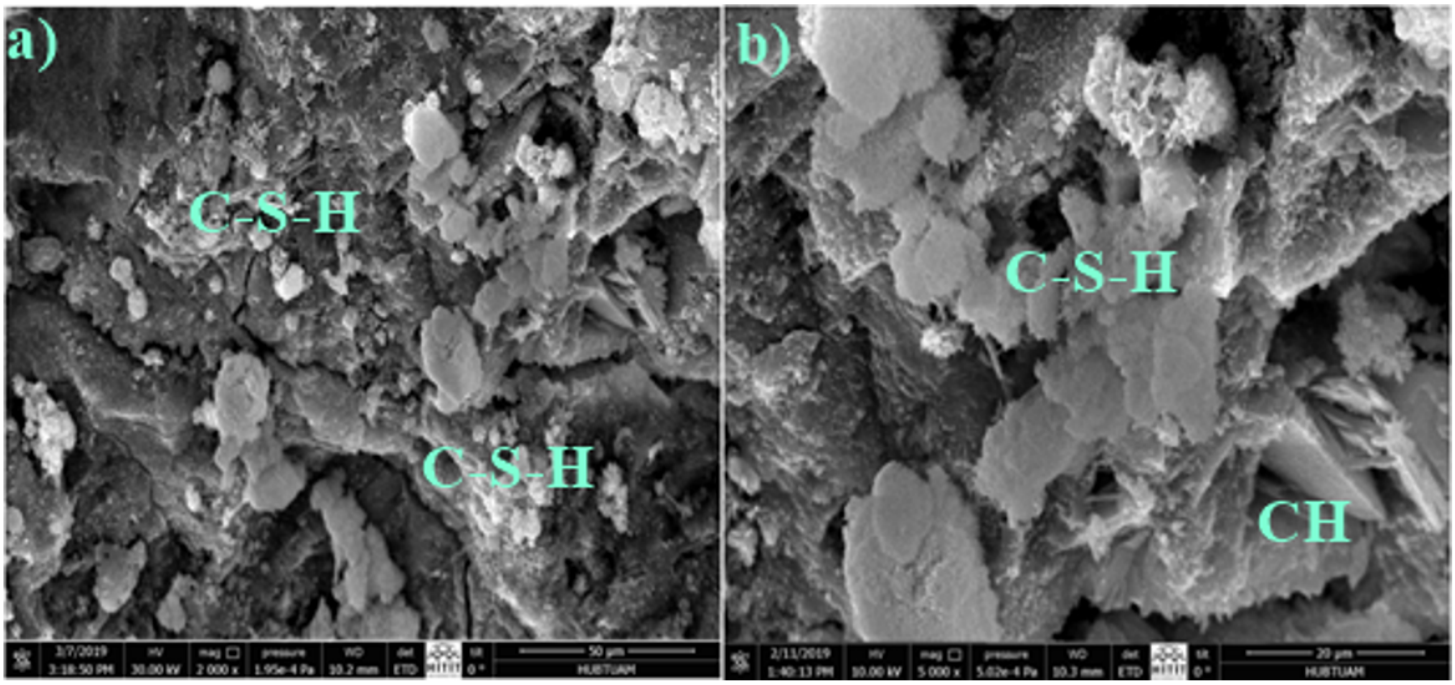

Figure 23

SEM images of samples having 20% BA at (a) 2000× (b) 5000× magnification at 28-days.

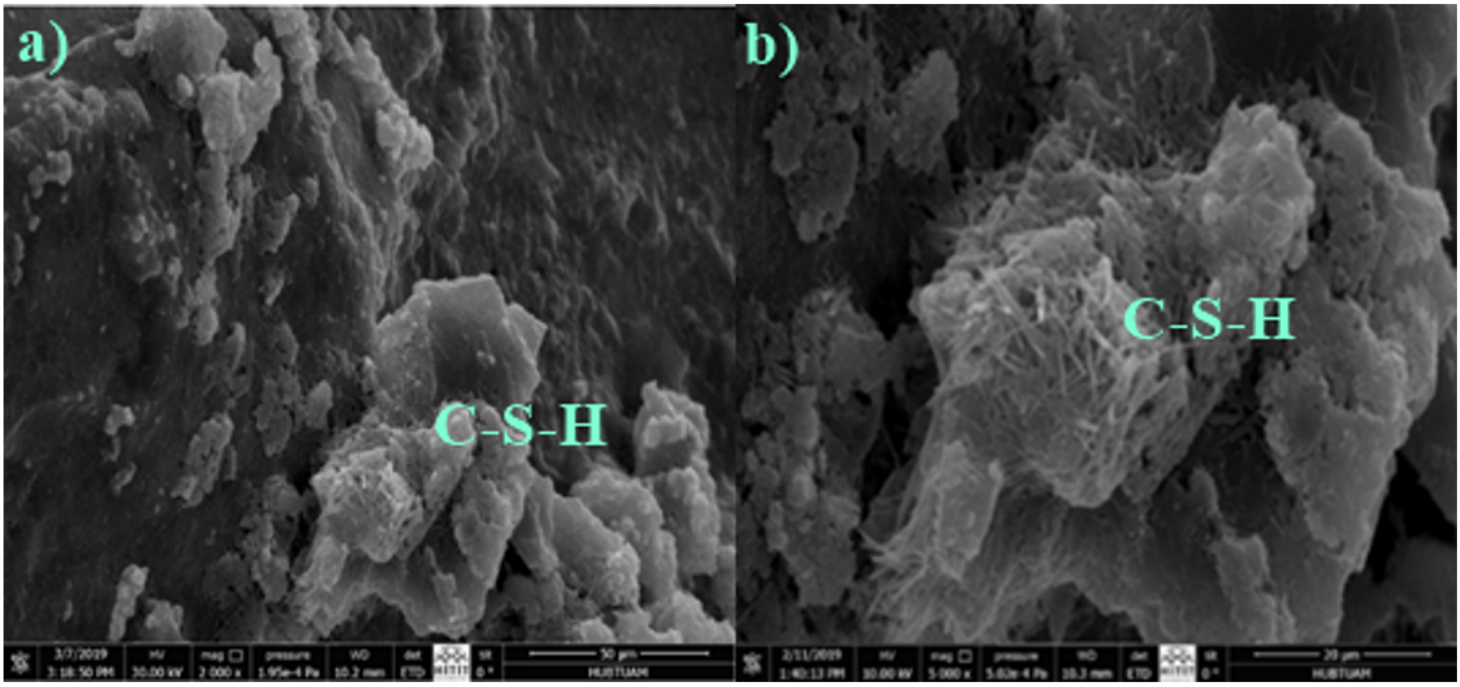

Figure 24

SEM images of samples having 20% BA at (a) 2000× (b) 5000× magnification at 90-days.